ACS APPLIED MATERIALS & INTERFACES

Research Article

www.acsami.org

# Asymmetric Response of Ferroelastic Domain-Wall Motion under Applied Bias

Michael L. Jablonski,[†] Shi Liu,[‡,§] Christopher R. Winkler,[†] Anoop R. Damodaran,[∥] Ilya Grinberg,[‡] Lane W. Martin,[∥,⊥] Andrew M. Rappe,[‡] and Mitra L. Taheri*[,†]

[†]Department of Materials Science and Engineering, Drexel University, Philadelphia, Pennsylvania 19104, United States

[‡]Department of Chemistry, University of Pennsylvania, Philadelphia, Pennsylvania 19104, United States

[∥]Department of Materials Science and Engineering, University of California, Berkeley, Berkeley, California 94720, United States

[⊥]Materials Science Division, Lawrence Berkeley National Laboratory, Berkeley, California 94720, United States

[§]Geophysical Laboratory, Carnegie Institution for Science, Washington, D.C. 20015, United States

**ABSTRACT:** The switching of domains in ferroelectric and multiferroic materials plays a central role in their application to next-generation computer systems, sensing applications, and memory storage. A detailed understanding of the response to electric fields and the switching behavior in the presence of complex domain structures and extrinsic effects (e.g., defects and dislocations) is crucial for the design of improved ferroelectrics. In this work, in situ transmission electron microscopy is coupled with atomistic molecular dynamics simulations to explore the response of 71° ferroelastic domain walls in $BiFeO_3$ with various orientations under applied electric-field excitation. We observe that 71° domain walls can have intrinsically asymmetric responses to opposing biases. In particular, when the electric field has a component normal to the domain wall, forward and backward domain-wall velocities can be dramatically different for equal and opposite fields. Additionally, the presence of defects and dislocations can strongly affect the local switching behaviors through pinning or nucleation of the domain walls. These results offer insight for controlled ferroelastic domain manipulation via electric-field engineering.

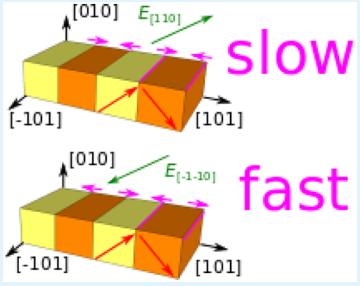


**KEYWORDS:** *bismuth ferrite, multiferroic, in situ, domain switching, ferroelectric*

## INTRODUCTION

Multiferroic materials exhibit intrinsic coupling between magnetic and electric order parameters,[1] allowing for their application in electronic and spintronic devices[2] such as magnetoelectronic sensors,[3] random access memories,[4] and high-density data storage devices.[5] The realization of multiferroic-based applications depends on the polarization switching process achieved through domain-wall motion driven by external electric fields.[1,6] Among single-phase multiferroics, one of the most promising materials for room-temperature device applications[9,10] is bismuth ferrite ($BiFeO_3$), a rhombohedral perovskite exhibiting both ferroelectricity and antiferromagnetism at room temperature.[7,8] In order to take advantage of complex materials such as $BiFeO_3$ in devices, a detailed understanding of the kinetics and dynamics of the ferroelectric switching process is required. To date, the majority of work on nanoscale ferroelectric switching in $BiFeO_3$ has focused on the local switching process of ferroelastic domain variants (71° and 109°) in thin films under an inhomogeneous electric field applied by a conductive tip on top of the sample as opposed to homogeneous (or globally) induced switching, which occurs in capacitor-based structures like those utilized in applicaitons.[11−15] Although these local probes have provided much insight and understanding of the local ferroelastic switching mechanism, exploration of the ferroelastic response on a global switching scale with high spatial and temporal resolution is still challenging. In particular, the response of ferroelastic domains in nanostructured films to a uniform opposing bias is not well understood.

The need for such studies is exacerbated by the ferroelastic switching process in thin films which is a complex interplay between intrinsic and extrinsic parameters such as domain structures,[16−18] epitaxial strain,[19] film thickness[20] and orientation,[21,22] applied voltage and sweep direction,[13] domain morphology,[23] defects,[24−26] and interfaces[27] (to name just a few factors to be considered). In particular, the presence of point defects[24−31] and dislocations[32−35] can have a profound impact on the domain-wall motion. The interactions between the ferroelastic domains in $BiFeO_3$ and point defects and dislocations have been studied by transmission electron microscopy (TEM).[26,27,30] These defects directly affect the nucleation and relaxation of ferroelastic domains by providing a local electrostatic potential that can both pin[25] and/or assist[24] the domain-wall motion. At the same time, the stress field coupled with the dislocations can drastically change the local polarization,[28] resulting in a significant barrier for domain-wall motion.[32−35] It is therefore imperative to decouple the effects

Received: September 4, 2015
Accepted: December 23, 2015
Published: December 23, 2015





DOI: 10.1021/acsami.5b08312
ACS Appl. Mater. Interfaces 2016, 8, 2935−2941

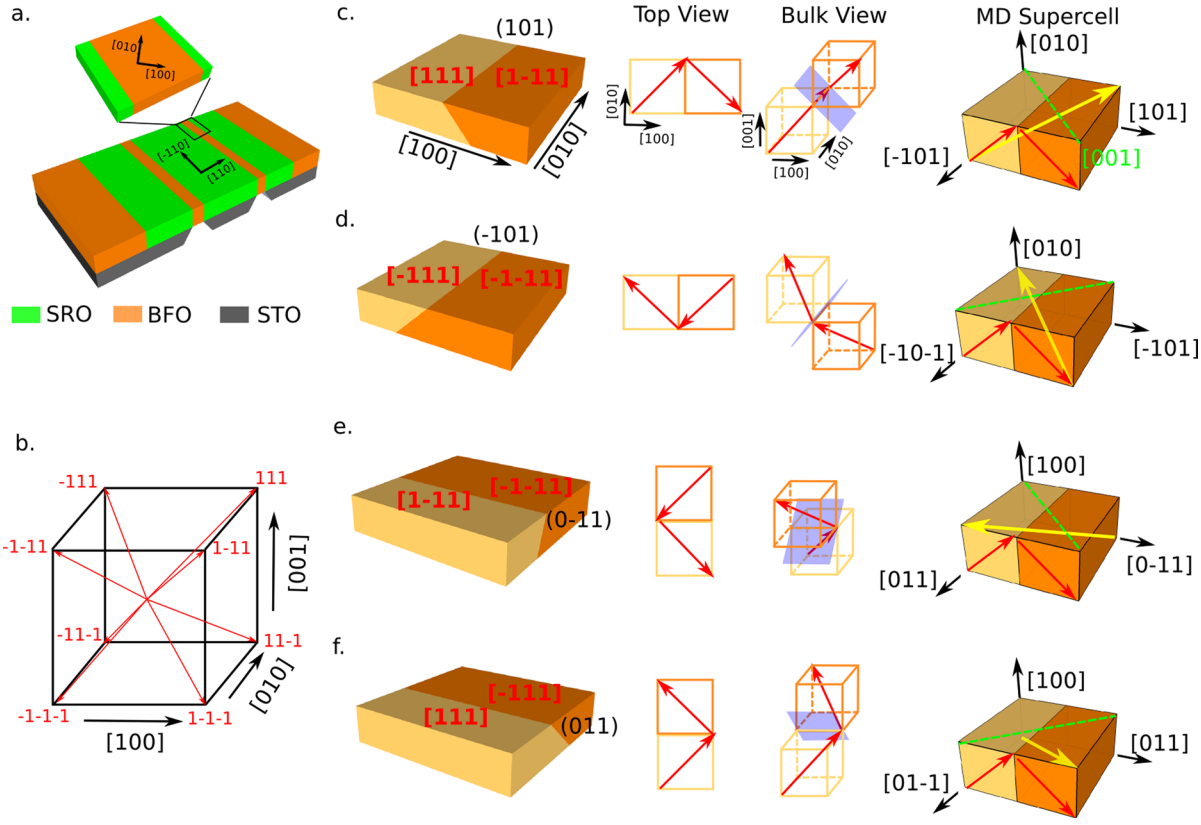


**Figure 1.** Ferroelastic 71° domain walls in $BiFeO_3$. (a) Device geometry for in situ biasing, showing the $SrRuO_3$ (SRO) electrode, $BiFeO_3$ film with surface normal along [001], and $SrTiO_3$ substrate. (b) Possible directions of the polarization vector of $BiFeO_3$ in a pseudocubic unit cell. (c) Schematic of a 71° domain wall in the (101) plane. The polarization vector changes from [111] to [1−11] across the domain wall. From left to right are shown a 3D model of a film with the 71° domain wall lying in the (101) plane, top view of the domain structure, bulk view of the domain structure, and the supercell used in MD simulations. The red arrow represents the polarization vector. The yellow arrow represents the electric field along the [110] direction. The broken green line shows the [001] axis. (d–f) 71° domain walls in the (−101), (0−11), and (011) planes, respectively.

resulting from these parameters to achieve a deep understanding of ferroelastic switching.

## EXPERIMENTAL AND MODELING PROCEDURE

In this work, we investigate the electric-field-induced response of ferroelastic 71° domain-wall structures in $BiFeO_3$ thin films during global switching via a combination of in situ TEM and atomistic molecular dynamics (MD) simulations.[36−38] This domain-wall variant grown on $SrTiO_3$ was chosen because of its ease of growth and demonstrated coupling to multiferroic behavior and as a continuation of previous experimental work by the authors.[26,30,31] Bias is applied via embedded $SrRuO_3$ electrodes along [110] as described in previous work, with the bias applied 45° to the long axes of the domain variants present.[26,30,31] The bias-direction dependence of the domain-wall motion and the influence of zero- and one-dimensional defects are examined experimentally, while MD simulations explore the intrinsic response of defect-free ferroelastic domains under opposing bias. By a comparison of the theoretical and experimental results, the intrinsic switching behavior and the influence of defects and dislocations on the response of ferroelastic domains can be decoupled and elucidated. We demonstrate that 71° domain walls in (001)-oriented thin films can have an asymmetric intrinsic response to opposing biases along [110], depending on the relative orientation of the different polarization variants on either side of the domain wall to the field direction. By applying an electric field with a component perpendicular to the switching polarization, one can effectively modulate the switching field and switching reversibility. In the presence of defects and dislocations, however, such local asperities can dominate the local switching behavior particularly in the case where dislocations intersect perpendicularly to the long axis of the domain.

## RESULTS AND DISCUSSION

MD simulations were designed such that they model the switching behavior of $BiFeO_3$ for fields applied along [110]. Using a bond-valence model described in the Methods section, the energies required to switch 71° domain-wall variants under both [110] and [−1−10] biases were determined. Experimental studies were subsequently designed to emulate and compliment the simulated domain structures by focusing on $BiFeO_3$ /$SrRuO_3$/$SrTiO_3$ (001) heterostructures prepared using pulsed-laser deposition (see the Methods section for details) with in-plane electrode structures designed to allow for the application of electric fields along [110] (Figure 1a). All polarization vectors are pointed along ⟨111⟩, with the experimentally relevant polarizations pointed toward the bottom of the crystal (Figure 1b). In turn, this geometry enables real-time observation of ferroelastic switching processes of domain structures in the entire device in situ under symmetric electric boundary conditions, eliminating the effects associated with tip shapes encountered in traditional scanning-probe measurements.[26,30,31] Previous studies reveal that 71°


DOI: 10.1021/acsami.5b08312
ACS Appl. Mater. Interfaces 2016, 8, 2935−2941

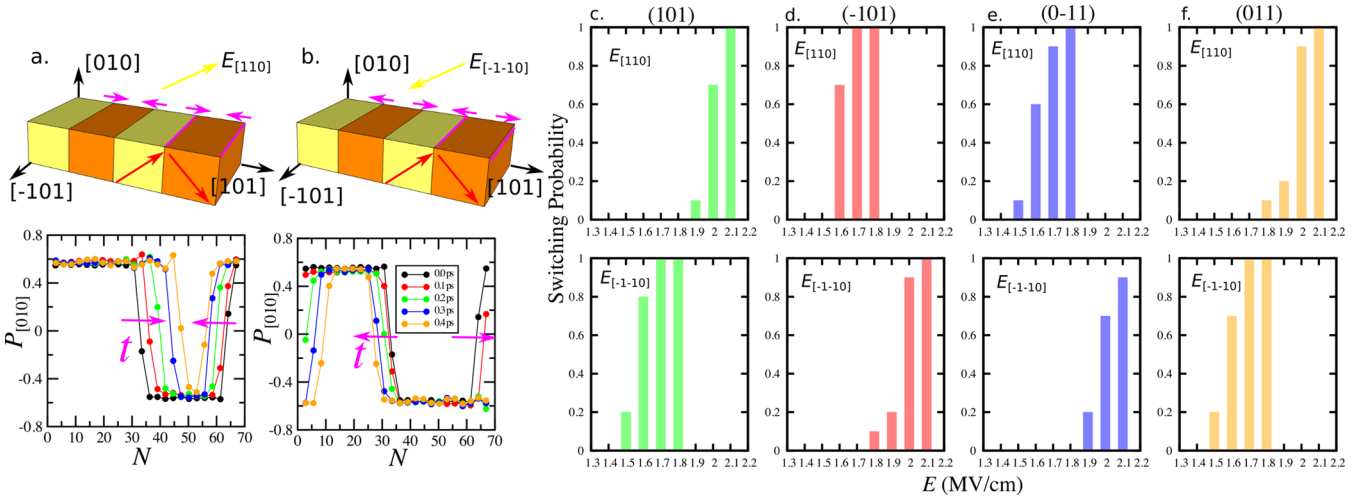


**Figure 2.** MD simulations of 71° domain-wall motions. (a) Simulated (101) 71° domain-wall motion under the [110] electric field. Top: schematic of domain-wall motion. Bottom: evolution of the polarization profiles. (b) Simulated (101) 71° domain-wall motion under the [−1−10] electric field. Field-dependent switching probability for (c) (101), (d) (−101), (e) (0−11), and (f) (011) 71° domain walls under the [110] and [−1−10] electric fields. The purple arrows denote the directions of domain-wall motion.

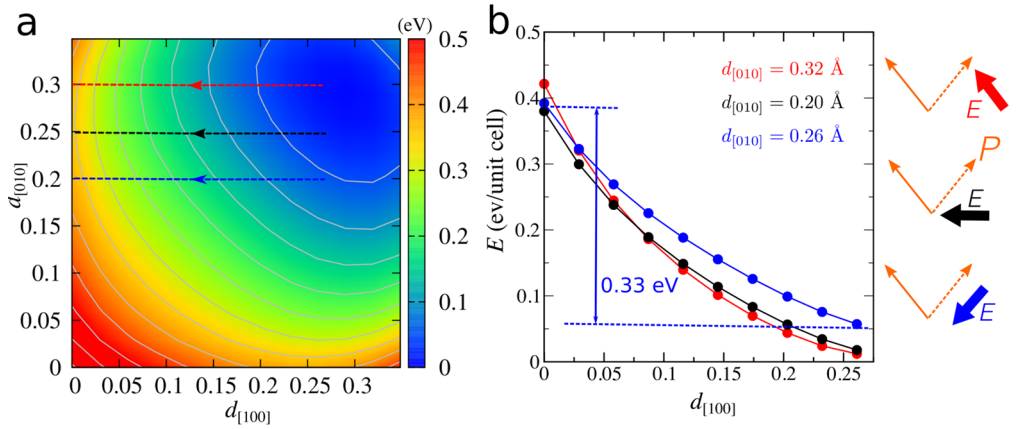


**Figure 3.** Lattice PES for 71° polarization rotation. (a) Lattice PES as a function of bismuth displacements along [100] and [010]. The lattice PES is constructed using the MD model potential, with the [001] component fixed at the ground-state value. The broken links denote three switching paths with different [010] atomic displacements. (b) Energy barriers for [111] → [−111] 71° switching with varying [010] atomic displacement. The schematics show the orientations of the electric fields giving rise to the three switching paths. Atomic displacement is in units of angstroms.

domain structures form on 101-type planes, inclined at 45° with respect to the [001] surface normal.[31] The underlying switching mechanism can be understood by identifying the types of domain walls based on the shapes of the domains and their response predicted from MD simulations. Despite being crystallographically distinct, {101}- or {011}-type domain walls cannot be individually distinguished from their respective plane groups through TEM alone because of the geometry of imaging (i.e., plane view, looking at a projection through the film thickness from the top of the sample, Figure 1c–f). It can, however, be determined that the {101}-type domain walls form a line along the [010] crystal axis at the surface. Likewise, all {011}-type domain walls lie along the [100] crystal axis at the surface. Using this methodology and comparing to the modeling results, we were able to determine which domain-wall variants are associated with each domain.

The results of our simulations revealed that the relative orientation between 71° domain walls and the direction of the applied bias dictates the magnitude of the lowest electric field required for domain switching. Parts c–f of Figure 1 present the supercells used for constructing 71° domain walls in $BiFeO_3$: the domain walls lie in the (101), (−101), (0−11), and (011) planes, respectively. All domain walls are inclined at 45° with respect to [001], resembling the domain-wall orientations in the actual thin films. The stability of the domain walls under applied fields along [110] and [−1−10] is evaluated by determining the lowest electric field required to move the domain wall within 15 ps, $E_s$. To correctly capture the stochastic behavior of domain switching, we perform multiple simulations starting from different equilibrium structures for a given field. The value of $E_s$ is then determined based on the probability of domain switching. Figure 2 shows simulated 71° domain-wall motion mechanisms and the field dependence of the switching probability for (101), (−101), (0−11), and (011) domain walls. We found that the field orientation does not influence the switching mechanism. As illustrated in Figure 2a,b, the domain undergoes 71° switching with the [0−10] ([010]) component of the polarization switched to [010] ([0−10]) under the [110] ([−1−10]) electric field. Remarkably, we find that it is significantly more difficult to induce motion in some domain walls rather than the others under the same bias conditions based on their respective orientations. The (101)


DOI: 10.1021/acsami.5b08312
ACS Appl. Mater. Interfaces 2016, 8, 2935−2941

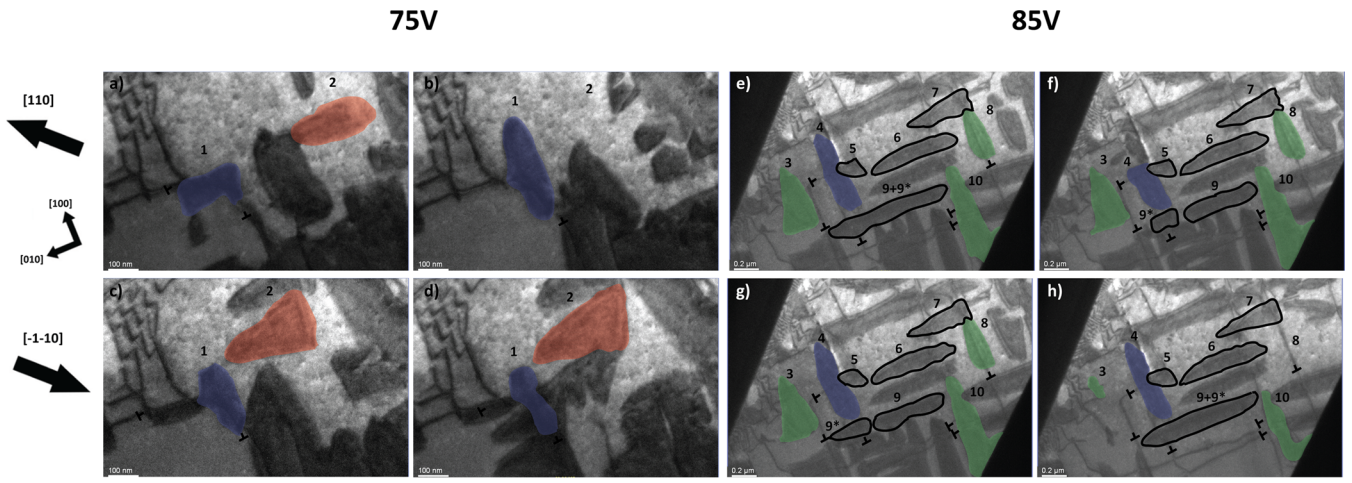


**Figure 4.** Series of frames extracted from in situ TEM videos ([110] applied bias on the top and [−1−10] applied bias on the bottom). For each set of frames, the left column (a and c) indicates the initial condition of domains, while the right column (b and d) indicates the final condition after biasing. Domains of note are outlined with walls identified (e−h) using the simulated results indicated with blue for (−101)/(−10−1), red for (01−1)/(011), and green for (101)/(10−1).

and (011) domain walls (Figure 2c,f) more easily undergo motion when the [−1−10] electric field is applied, while the (−101) and (0−11) domain walls (Figure2d,e) are more easily switched under the [110] electric field. Despite the application of an electric field to the cells being in a symmetric system, the overall response is dominated by the asymmetries in the energetics of switching the polarization vectors. This leads to the conclusion that the global domain response of a symmetric ferroelastic system is inherently asymmetric.

We also found that it is possible to tune the switching speed by engineering the relative orientation between the polarization and electric field. The bias dependence of the required switching field was further explored by constructing the lattice potential energy surface (PES) as a function of atomic displacements along [100] and [010]. An ideal direct 71° switching event involves the change of only one component of the atomic displacement (e.g., [100] → [−100]). From the lattice PES shown in Figure 3a, we found that the magnitude of the atomic displacement along [010] influences the energy required to achieve a 71° switching from [111] to [−111]. As demonstrated in Figure 3b, under a field that reduces the [010] atomic displacement, the 71° switching path from [100] to [−100] has a lower energy barrier.

Moreover, by applying an electric field with a component that is perpendicular to the switching polarization component and oriented such that it reduces the overall dipole magnitude, the barrier for switching can be reduced. Specifically, the [010] component of the [110] electric field, although not directly contributing to the switching of the [100] component of the dipole from [111] to [−111], will influence polarization across the domain wall along [010] and thus affect the height of the energy barrier for switching. Therefore, we find that 71° domain walls have an asymmetric response to in-plane bias ([110] and [−1−10]) depending on the wall orientation with respect to the field. Hence, we predict that under bias along [110], the (−101), (−10−1), (0−11), and (0−1−1) domain-wall types undergo motion more easily than the other 71° domain walls. Likewise, under [−1−10] bias, the (101), (10−1), (011), and (01−1) domain-wall types more readily undergo motion. Applying an electric field purely along the switching polarization component will recover the reversibility of domain-wall motion.

In direct comparison to the MD simulations, in situ biasing using TEM shows that domains respond asymmetrically under positive and negative biases. By distinguishing the crystallographic directions along which specific domain-wall variants can exist and using the interactions of the domains with applied bias predicted by the above model, we determine which domain wall types are present. Under bias along [110], we observe domains with majority walls of (0−11)/(0−1−1) and (01−1)/(011) to undergo motion, while under negative bias, domains with majority walls of (101)/(10−1) also undergo motion. These results are in direct agreement with the asymmetric response predicted by the MD simulations. Using the crystallographic domain-wall determination methodology as described above, we see that domain-wall variants of (0−11)/(0−1−1), specifically Domain 1 (Figure 4), undergo growth along [010] while exposed to positive bias. This event occurs despite the presence of a dislocation inside the bulk of the domain. Likewise, (01−1)/(011) domain-wall variants, Domain 2 (Figure 4), tended to shrink under positive bias. On a wider scale, domain motion was also observed for domain-wall variants of (101)/(10−1) under negative bias (Figure 4) with Domains 3, 8, and 10. While all of these domains undergo motion, there is deviation from the predicted behavior once defects are encountered, such as dislocations in the cases of Domains 3 and 10.

While in general the experimental results followed closely with the MD simulations, there were several anomalous domain behaviors that occurred mostly influenced by the presence of defects. Despite the common belief of dislocations globally acting as pinning sites and the authors' previous work indicating that dislocations can globally affect the switching behavior, our observations reveal that only certain dislocation orientations affect the local domain-wall motion.[26] Specifically, dislocations running through the long axis (see Domain 8 in Figure 4) do not seem to have a noticeable effect, while perpendicular dislocations (see Domain 3, 4, and 7 in Figure 4) appear to influence it greatly. Cartoon schematics showing the idealized domain motion along with the effects of nonidealized cases with dislocations at orientations are shown to help guide the


DOI: 10.1021/acsami.5b08312
ACS Appl. Mater. Interfaces 2016, 8, 2935−2941

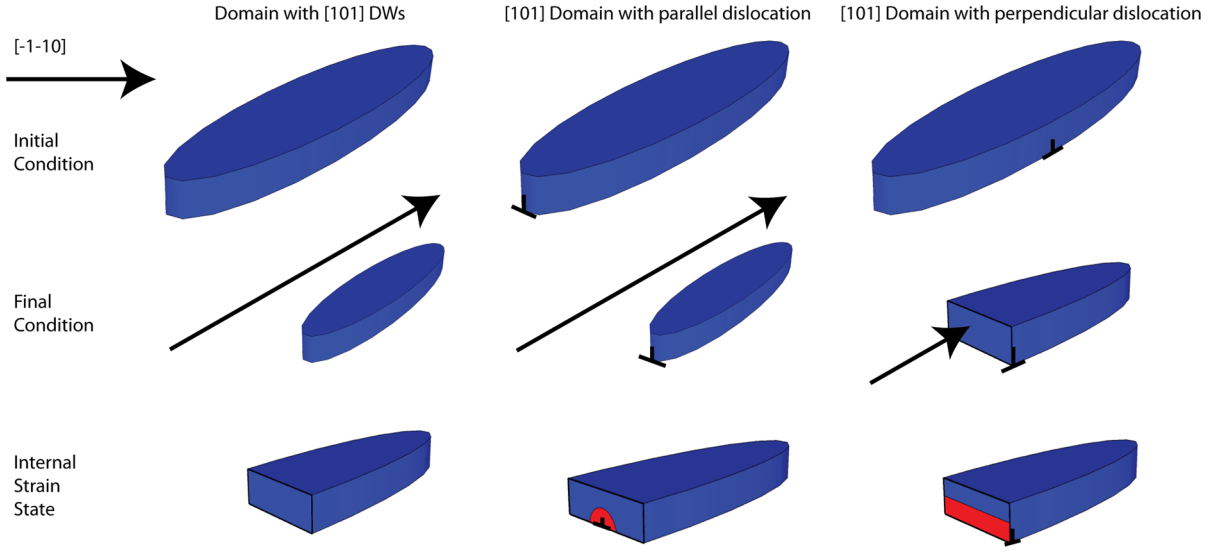


**Figure 5.** Cartoon schematic showing the typical domain response of a (101) domain under [−1−10] bias in the presence of no defects (left), a dislocation running through the domain's long axis (middle), and a dislocation running perpendicular to the domain's long axis (right). Arrows indicate the extent of domain motion in these conditions, while the exaggerated strain state on the moving domain wall caused by the dislocation is indicated in red. Domains walls are not inclined for ease of interpretation.

eye (Figure 5). The localized electrostatic potential and lattice strain induced by dislocations can influence the domain walls, and the differing types and proximities are likely the root of these differing behaviors. As the domain tip recedes from the direction of applied bias with a dislocation parallel to its long axis, the domain wall only interacts with a small area affected by the dislocation (Figure 5). In this case, it is very similar to previous work done using phase field simulations to predict the nucleation and growth of a domain; however, in this case, the behavior is reversed.[26] On the other hand, in the perpendicular case, the receding domain tip interacts with a much larger area of lattice influenced by the dislocation. As such, the pinning effect of the dislocation is more pronounced because of a larger interaction area (Figure 5). In addition to the deviations from predicted behavior caused by the presence of dislocations perpendicular to the domain long axis, several domains had anomalous behavior unassociated with visible dislocations. While oriented with domains in {011}, Domain 6 underwent no motion in either positive or reverse bias. This indicates that there is an underlying pinning mechanism caused by either domain−domain or domain−defect interactions that are unobservable under the current imaging conditions. While having the same orientation and general shape as Domain 6, Domains 9 and 9* separated into two domains under positive bias and recombined under negative bias. This deviation from expected behavior is due to factors that are not visible in the current imaging conditions, perhaps mitigated by point defects or dislocations in a different diffracting condition. Particularly small domains such as Domain 5, where the majority domain-wall variant cannot be distinguished, seemed to remain stable under both positive and negative biases as well. This seems to be caused by the domain walls native to the domain itself competing against each other and thus providing a self-pinning mechanism. The anomalous effects observed during this study will require further analysis using both simulations and direct strain measurements through TEM in order to be fully understood.

From these direct observations, it is apparent that while in many cases the overall behavior occurs as predicted by the above model, there exists asymmetry to the ferroelastic response based on the domain-wall and electric-field orientations. In addition to the asymmetry caused by the energetics of the polarization switching path, more localized deviations are found to be caused by defects, specifically dislocations, as has been previously reported.[26] Traditionally, merely the presence of dislocations inside a domain was believed to be enough to pin a material, but like the direction dependence of the asymmetric response, it appears that the orientation of the dislocation itself dictates whether or not a domain will actually be pinned. Intuitively, the interaction volume of the strain field around a dislocation should provide the energy barrier needed to pin a domain wall, yet this is not observed using TEM in this study. Instead, the area strain field interacting with a receding domain tip plays the most significant role in determining whether a domain will be pinned or not schematically shown in Figure 5. While the dislocation running through Domain 8 has a larger interaction volume than those in Domains 3, 4, and 7, it does not pin the domain, whereas the larger interaction area from the dislocations running perpendicular to the domain long axis in Domains 3, 4, and 7 does pin the domains. These results indicate that care must be taken with both the orientation of the domains and the orientation of the dislocations introduced during the growth process when considering the feasibility of domain switching in a device structure.

## CONCLUSION

Using MD simulations and in situ TEM, we demonstrate that 71° domain walls in (001) thin films of $BiFeO_3$ can have asymmetric intrinsic responses to opposing biases along the [110] direction, depending on their crystallographic orientations relative to the field direction. It is found that applying an electric field with a component perpendicular to the switching polarization component modulates the magnitude of the switching field and switching reversibility. This suggests a novel route for controlled ferroelastic domain manipulation via electric-field engineering. We determine that globally domains respond to electrical bias in an intrinsic manner, as predicted by


DOI: 10.1021/acsami.5b08312
ACS Appl. Mater. Interfaces 2016, 8, 2935−2941

MD simulations. Defects and dislocations can significantly modulate the exact switching behaviors at the local scale, leading to minor inconsistencies despite the overall behavior following the model as predicted. The overall effect of dislocations does not alter to a large degree the switching behavior, only causing local instabilities and unpredictability to ferroelastic switching. In particular, dislocations running perpendicular to the long axes of domains can impede domain-wall motion. The effects of these defects can have a profound role on the mitigation of switching mechanisms in $BiFeO_3$ grown in this configuration. Removal and control of these defects through selection of the as-grown strain state on different substrates will lead to more predictable switching at the global and local levels. This work offers insight into the combined effects of domain-wall types, defect states, and orientation of the applied electric field on ferroelastic switching and can potentially lead to a more comprehensive understanding of ferroelastic switching in an environment and geometry that mimic realistic devices.

## METHODS

**Epitaxial Thin-Film Growth.** $BiFeO_3$ films used in this study were grown such that embedded epitaxial electrodes can be used to apply in-plane electric fields through connection to a voltage source. Starting with an (001)-oriented $SrTiO_3$ substrate, 75 nm $SrRuO_3$ electrodes were deposited using pulsed-laser deposition. Subsequently, ≈85 nm of $BiFeO_3$ was deposited over the surface of the sample, allowing for trenches of $BiFeO_3$ to form an epitaxial relationship with the substrate between the electrodes. As a result of this growth configuration, 71° domains were favored to form on the {101} family of planes.

**TEM.** In-plane biasing of the $BiFeO_3$ thin films was performed in the TEM, described in detail in refs 26, 30, and 31 with an applied bias along the [110] of the substrate. These experiments were carried out in both positive and negative biases, allowing for the reversibility of domain switching to be examined. The contrast between domains is caused by the diffraction contrast on individual domains captured by the camera as 256 shades of gray. A comparison of individual frames extracted from videos taken during in situ biasing yielded quantitative analysis of individual domains during both nucleation and relaxation.

**MD Simulations.** We carried out isothermal−isobaric (*NPT*) MD simulations to explore the ferroelastic response of 71° domain walls to the bias direction with an 11520-atom perovskite-type supercell using a bond-valence-based interatomic potential.[18,36−38] Simulations with a defect-free bulk $BiFeO_3$ supercell allow separation of the intrinsic response from those due to the surface and defects.[6] The interatomic potential used is parametrized from first-principles calculations and is able to reproduce the temperature-driven phase transition of bulk $BiFeO_3$ and density functional theory domain-wall energies accurately.[36] The speed of the domain wall is determined by the rate of change of the total polarization of the supercell. The instantaneous local polarization, $P_u(t)$, within each 5-atom unit cell is calculated with

$$P_u(t) = \frac{1}{V_u}\left[\frac{1}{8}\mathbf{Z}_{Bi}^{*}\cdot\sum_{i=1}^{8} r_{Bi,i}(t) + \mathbf{Z}_{Fe}^{*}\cdot r_{Fe}(t) + \frac{1}{2}\mathbf{Z}_{O}^{*}\cdot\sum_{i=1}^{6} r_{O,i}(t)\right]$$

where $V_u$ is the volume of a unit cell, $\mathbf{Z}_{Bi}^{*}$, $\mathbf{Z}_{Fe}^{*}$, and $\mathbf{Z}_{O}^{*}$ are the Born effective charge tensors, and $r_{Bi,i}(t)$, $r_{Fe}(t)$, and $r_{O,i}(t)$ are instantaneous atomic positions of Bi, Fe, and O atoms in a unit cell obtained from MD simulations. The instantaneous total polarization of the supercell is the sum of $P_u(t)$ divided by the number of unit cells.

## AUTHOR INFORMATION


### Corresponding Author

*E-mail: mtaheri@coe.drexel.edu.


### Author Contributions

The manuscript was written through contributions of all authors. All authors have given approval to the final version of the manuscript.


### Funding

M.L.T., M.L.J., and C.R.W. acknowledge support of the Office of Naval Research under Contract N00014-1101-0296. S.L. acknowledges support from the National Science Foundation under Grant DMR-1124696 and support from the Carnegie Institution for Science. I.G. acknowledges support from the Office of Naval Research under Grant N00014-12-1-1033. A.R.D. acknowledges support from the Army Research Office under Grant W911NF-14-1-0104. L.W.M. acknowledges support from the National Science Foundation under Grant DMR-1451219. A.M.R. acknowledges support from the Department of Energy under Grant DE-FG02-07ER46431. Aberration-corrected TEM experiments were performed in the Argonne National Laboratory's Electron Microscopy Center, supported by the Department of Energy's Office of Science. Electron microscopy experiments were conducted in Drexel University's Centralized Research Facilities. Computational support was provided by the High Performance Computing Modernization Program (HPCMO) of the U.S. DoD and by the National Energy Research Scientific Computing Center of the Department of Energy.


### Notes

The authors declare no competing financial interest.

## REFERENCES


(1) Ramesh, R.; Spaldin, N. A. Multiferroics: Progress and Prospects in Thin Films. *Nat. Mater.* **2007**, *6* (1), 21−29.

(2) Pantel, D.; Chu, Y.-H.; Martin, L. W.; Ramesh, R.; Hesse, D.; Alexe, M. Switching Kinetics in Epitaxial BiFeO3 Thin Films. *J. Appl. Phys.* **2010**, *107* (8), 4−7.

(3) Ma, J.; Hu, J.; Li, Z.; Nan, C.-W. Recent Progress in Multiferroic Magnetoelectric Composites: From Bulk to Thin Films. *Adv. Mater.* **2011**, *23* (9), 1062−1087.

(4) Scott, J. F. Multiferroic Memories. *Nat. Mater.* **2007**, *6* (April), 256−257.

(5) Scott, J. F. Applications of Modern Ferroelectrics. *Science* **2007**, *315* (5814), 954−959.

(6) Liu, S.; Grinberg, I.; Rappe, A. M. Exploration of the Intrinsic Inertial Response of Ferroelectric Domain Walls via Molecular Dynamics Simulations. *Appl. Phys. Lett.* **2013**, *103* (23), 232907.

(7) Bhide, V. G.; Multani, M. S. Mossbauer effect in ferroelectric-antiferromagnetic BiFeO3. *Solid State Commun.* **1965**, *3*, 271−274.

(8) Moreau, J.; Michel, C.; Gerson, R.; James, W. Ferroelectric BiFeO3 X-Ray and Neutron Diffraction Study. *J. Phys. Chem. Solids* **1971**, *32* (6), 1315−1320.

(9) Catalan, G.; Scott, J. F. Physics and Applications of Bismuth Ferrite. *Adv. Mater.* **2009**, *21* (24), 2463−2485.

(10) Young, S. M.; Zheng, F.; Rappe, A. M. First-Principles Calculation of the Bulk Photovoltaic Effect in Bismuth Ferrite. *Phys. Rev. Lett.* **2012**, *109* (23), 236601.

(11) Chu, Y.-H.; Martin, L. W.; Holcomb, M. B.; Gajek, M.; Han, S.-J.; He, Q.; Balke, N.; Yang, C.-H.; Lee, D.; Hu, W.; Zhan, Q.; Yang, P.-L.; Fraile-Rodríguez, A.; Scholl, A.; Wang, S. X.; Ramesh, R. Electric-Field Control of Local Ferromagnetism Using a Magnetoelectric Multiferroic. *Nat. Mater.* **2008**, *7* (6), 478−482.

(12) Balke, N.; Choudhury, S.; Jesse, S.; Huijben, M.; Chu, Y. H.; Baddorf, a P.; Chen, L. Q.; Ramesh, R.; Kalinin, S. V. Deterministic Control of Ferroelastic Switching in Multiferroic Materials. *Nat. Nanotechnol.* **2009**, *4* (12), 868−875.

(13) Béa, H.; Ziegler, B.; Bibes, M.; Barthélémy, a; Paruch, P. Nanoscale Polarization Switching Mechanisms in Multiferroic $BiFeO_3$ Thin Films. *J. Phys.: Condens. Matter* **2011**, *23* (14), 142201.




DOI: 10.1021/acsami.5b08312
*ACS Appl. Mater. Interfaces* 2016, 8, 2935−2941

(14) Kim, Y.; Han, H.; Lee, W.; Baik, S.; Hesse, D.; Alexe, M. Non-Kolmogorov-Avrami-Ishibashi Switching Dynamics in Nanoscale Ferroelectric Capacitors. *Nano Lett.* **2010**, *10* (4), 1266−1270.
(15) Mazumdar, D.; Shelke, V.; Iliev, M.; Jesse, S.; Kumar, A.; Kalinin, S. V.; Baddorf, A. P.; Gupta, A. Nanoscale Switching Characteristics of Nearly Tetragonal BiFeO3 Thin Films. *Nano Lett.* **2010**, *10* (7), 2555−2561.
(16) Nagarajan, V.; Roytburd, a; Stanishevsky, a; Prasertchoung, S.; Zhao, T.; Chen, L.; Melngailis, J.; Auciello, O.; Ramesh, R. Dynamics of Ferroelastic Domains in Ferroelectric Thin Films. *Nat. Mater.* **2003**, *2* (1), 43−47.
(17) Aravind, V. R.; Morozovska, a. N.; Bhattacharyya, S.; Lee, D.; Jesse, S.; Grinberg, I.; Li, Y. L.; Choudhury, S.; Wu, P.; Seal, K.; Rappe, a. M.; Svechnikov, S. V.; Eliseev, E. a.; Phillpot, S. R.; Chen, L. Q.; Gopalan, V.; Kalinin, S. V. Correlated Polarization Switching in the Proximity of a 180° Domain Wall. *Phys. Rev. B: Condens. Matter Mater. Phys.* **2010**, *82* (2), 1−11.
(18) Shin, Y.; Grinberg, I.; Chen, I.; Rappe, A. Nucleation and Growth Mechanism of Ferroelectric Domain-Wall Motion. *Nature* **2007**, *449*, 881.
(19) Gao, P.; Nelson, C. T.; Jokisaari, J. R.; Baek, S.-H.; Bark, C. W.; Zhang, Y.; Wang, E.; Schlom, D. G.; Eom, C.-B.; Pan, X. Revealing the Role of Defects in Ferroelectric Switching with Atomic Resolution. *Nat. Commun.* **2011**, *2*, 591.
(20) Cillessen, J. F. M.; Prins, M. W. J.; Wolf, R. M. Thickness Dependence of the Switching Voltage in All-Oxide Ferroelectric Thin-Film Capacitors Prepared by Pulsed Laser Deposition. *J. Appl. Phys.* **1997**, *81*, 2777.
(21) Xu, R.; Karthik, J.; Damodaran, A. R.; Martin, L. W. Stationary Domain Wall Contribution to Enhanced Ferroelectric Susceptibility. *Nat. Commun.* **2014**, *5*, 1−7.
(22) Xu, R.; Liu, S.; Grinberg, I.; Karthik, J.; Damodaran, A. R.; Rappe, A. M.; Martin, L. W. Ferroelectric Polarization Reversal via Successive Ferroelastic Transitions. *Nat. Mater.* **2014**, *14* (1), 79−86.
(23) Shelke, V.; Srinivasan, G.; Gupta, A. Ferroelectric Properties of BiFeO 3 Thin Films Deposited on Substrates with Large Lattice Mismatch. *Phys. Status Solidi RRL* **2010**, *4* (3−4), 79−81.
(24) Jesse, S.; Rodriguez, B. J.; Choudhury, S.; Baddorf, A. P.; Vrejoiu, I.; Hesse, D.; Alexe, M.; Eliseev, E. a; Morozovska, A. N.; Zhang, J.; Chen, L.-Q.; Kalinin, S. V. Direct Imaging of the Spatial and Energy Distribution of Nucleation Centres in Ferroelectric Materials. *Nat. Mater.* **2008**, *7* (3), 209−215.
(25) Yang, C.-H.; Kan, D.; Takeuchi, I.; Nagarajan, V.; Seidel, J. Doping BiFeO3: Approaches and Enhanced Functionality. *Phys. Chem. Chem. Phys.* **2012**, *14* (46), 15953−15962.
(26) Winkler, C.; Jablonski, M.; Ashraf, K. Real-Time Observation of Local Strain Effects on Non-Volatile Ferroelectric Memory Storage Mechanisms. *Nano Lett.* **2014**, *14* (6), 3617−3622.
(27) Nelson, C. T.; Gao, P.; Jokisaari, J. R.; Heikes, C.; Adamo, C.; Melville, A.; Baek, S.; Folkman, C. M.; Winchester, B.; Gu, Y.; Liu, Y.; Zhang, K.; Wang, E.; Li, J.; Chen, L. Domain Dynamics During Ferroelectric Switching. *Science (Washington, DC, U. S.)* **2011**, *334*, 968−971.
(28) Alpay, S. P.; Misirlioglu, I. B.; Nagarajan, V.; Ramesh, R. Can Interface Dislocations Degrade Ferroelectric Properties? *Appl. Phys. Lett.* **2004**, *85* (11), 2044.
(29) Lubk, A.; Rossell, M. D.; Seidel, J.; He, Q.; Yang, S. Y.; Chu, Y. H.; Ramesh, R.; Hÿtch, M. J.; Snoeck, E. Evidence of Sharp and Diffuse Domain Walls in BiFeO3 by Means of Unit-Cell-Wise Strain and Polarization Maps Obtained with High Resolution Scanning Transmission Electron Microscopy. *Phys. Rev. Lett.* **2012**, *109* (4), 047601.
(30) Winkler, C. R.; Damodaran, A. R.; Karthik, J.; Martin, L. W.; Taheri, M. L. Direct Observation of Ferroelectric Domain Switching in Varying Electric Field Regimes Using in Situ TEM. *Micron* **2012**, *43* (11), 1121−1126.
(31) Winkler, C. R.; Jablonski, M. L.; Damodaran, A. R.; Jambunathan, K.; Martin, L. W.; Taheri, M. L. Accessing Intermediate Ferroelectric Switching Regimes with Time-Resolved Transmission Electron Microscopy. *J. Appl. Phys.* **2012**, *112* (5), 052013.
(32) Lubk, A.; Rossell, M. D.; Seidel, J.; Chu, Y. H.; Ramesh, R.; Hÿtch, M. J.; Snoeck, E. Electromechanical Coupling among Edge Dislocations, Domain Walls, and Nanodomains in BiFeO3 Revealed by Unit-Cell-Wise Strain and Polarization Maps. *Nano Lett.* **2013**, *13* (4), 1410−1415.
(33) Chu, M.-W.; Szafraniak, I.; Scholz, R.; Harnagea, C.; Hesse, D.; Alexe, M.; Gösele, U. Impact of Misfit Dislocations on the Polarization Instability of Epitaxial Nanostructured Ferroelectric Perovskites. *Nat. Mater.* **2004**, *3* (2), 87−90.
(34) Emelyanov, A. Y.; Pertsev, N. A. Abrupt Changes and Hysteretic Behavior of 90° Domains in Epitaxial Ferroelectric Thin Films with Misfit Dislocations. *Phys. Rev. B: Condens. Matter Mater. Phys.* **2003**, *68* (21), 214103.
(35) Su, D.; Meng, Q.; Vaz, C. a. F.; Han, M.-G.; Segal, Y.; Walker, F. J.; Sawicki, M.; Broadbridge, C.; Ahn, C. H. Origin of 90° Domain Wall Pinning in Pb(Zr0.2Ti0.8)O3 Heteroepitaxial Thin Films. *Appl. Phys. Lett.* **2011**, *99* (10), 102902.
(36) Liu, S.; Grinberg, I.; Rappe, A. M. Development of a Bond-Valence Based Interatomic Potential for BiFeO3 for Accurate Molecular Dynamics Simulations. *J. Phys.: Condens. Matter* **2013**, *25* (10), 102202.
(37) Liu, S.; Grinberg, I.; Takenaka, H.; Rappe, A. M. Reinterpretation of the Bond-Valence Model with Bond-Order Formalism: An Improved Bond-Valence-Based Interatomic Potential for PbTiO3. *Phys. Rev. B: Condens. Matter Mater. Phys.* **2013**, *88* (10), 104102.
(38) Shin, Y.-H.; Cooper, V.; Grinberg, I.; Rappe, A. Development of a Bond-Valence Molecular-Dynamics Model for Complex Oxides. *Phys. Rev. B: Condens. Matter Mater. Phys.* **2005**, *71* (5), 054104.


DOI: 10.1021/acsami.5b08312
*ACS Appl. Mater. Interfaces* 2016, 8, 2935−2941